Model Predictive Valve Control to Assist Lung Pressure Profile Tracking

M. C. Thompson, C. T. Freeman, N. O'Brien, A.-M. Hughes, R. Marchbanks, A. Birch

***Abstract*—In the UK 60,000 people have a brain tumour, and typically are unaware of its presence until symptoms occur. Currently there is no mass screening available due to limitations in diagnostic techniques. Measurement of intracranial pressure (via tympanic membrane displacement) is a potential low-cost, accessible solution, however pressure fluctuations degrade its accuracy. This paper develops a solution to this problem by assisting participants to precisely track airway pressure profiles. This stabilises intrathoracic pressure, significantly reducing the fluctuations and enabling accurate diagnosis of intracranial pressure.**

The paper develops and evaluates the first model of lung pressure tracking to embed volitional control action. A clinically feasible identification approach is then derived, together with a novel model predictive control framework, embedding a valve control subsystem. Results with 10 participants confirm that tracking is improved by an average of 22%.

***Index Terms*—intracranial pressure, brain tumour, airway pressure tracking, model predictive control, diagnostics**

I. Introduction

NEUROLOGICAL conditions affect 11 million people in the UK (around 1 in 6 people), account for 800,000 hospital admissions every year, and cause 1 in 5 deaths [1]. Approximately 70% of these deaths were attributed to conditions that affect the anatomy of the brain such as tumours or cerebral haemorrhage [2]. Early identification of intracranial pathologies can increase the available treatment options and dramatically improve the chance of long-term survival. Current non-invasive methods for identifying cranial pathologies comprise magnetic resonance imaging, computerised tomography, and brain electrical activity (e.g. magnetoencephalography and electroencephalography). However, they all require highly specialised and expensive equipment, making their application in mass screening by general practitioners unfeasible. Therefore a new approach is needed for early diagnosis of cranial pathologies.

A. Intracranial Pressure Measurement

Pressure in the neurocranium is known as intracranial pressure (ICP), and must remain within closely maintained limits to ensure the brain functions properly. ICP cannot be used to identify the cause of neurological conditions but instead characterises the overall state of health of the brain and can be used to identify whether any pathologies are present. Changes in ICP can cause constriction of blood vessels and, if left untreated, lead to hypoxia and the death of brain tissue. Cerebral blood flow regulation and cerebrospinal fluid regulation usually maintain ICP within a fixed range (7–15 mmHg) even when changes occur in the body, e.g. increased blood flow due to exercise or age related anatomical changes in the brain. However, these regulatory mechanisms break down when significant pathologies such as tumours are present. The ability to measure ICP non-invasively and accurately would provide an accessible, low cost solution to the diagnosis of cranial malfunction.

A potential non-invasive, accessible solution to intracranial pressure measurement has recently been proposed by researchers at University Hospital Southampton (UHS). They used a cerebral and cochlear fluid pressure (CCFP) analyser to show that there is a fluid link between the inner ear and cerebrospinal fluid [3]. They then demonstrated that movement of the eardrum can be measured using acoustic reflex stimulation based tympanic membrane displacement (TMD) to indirectly yield the pressure in the inner ear. TMD profiles comprise audio stimulation applied over intervals of about 20 seconds.

Several other research programmes have investigated TMD as a non-invasive measure of ICP [3]–[6]. Their main conclusions are that it is a plausible solution but measurements are corrupted by fluctuations in pressure due to cardiac and respiratory processes which affect cerebral blood flow regulation. Cerebral blood flow regulation is affected by airway pressure [7]–[13] via multiple mechanisms in the body which link intrathoracic pressure with ICP [14]. The practical consequence of these interactions is that pressure fluctuations can be mitigated by measuring and precisely controlling airway/thoracic pressure during TMD measurements.

The standard experimental approach to control intrathoracic pressure used in numerous studies requires participants to blow into a tube (forced exhalation) in order to generate specific pressures at specific time intervals. This is called lung pressure profiling and is used to observe how thoracic and cardiac pressures affect ICP. These profiles, displayed on a screen, typically comprise square waves, sine waves or a sequence of step changes which the participant is required to track accurately. The closer these profiles are tracked, the better the comparative data for ICP measurements. Unfortunately, participants find it is inherently difficult to precisely control their lung pressure during forced exhalation tests.

This work was supported by the U.K. Engineering and Physical Sciences Research Council.

M. C. Thompson and C. T. Freeman are with the School of Electronics and Computer Science, University of Southampton, Southampton SO17 1BJ, U.K. (email: mt10g17@soton.ac.uk; cf@ecs.soton.ac.uk)

A.-M. Hughes is with the School of Health Sciences, University of Southampton, Southampton SO17 1BJ, U.K. (email: a.hughes@soton.ac.uk)

N. O'Brien, R. Marchbanks and A. Birch are with the Department of Medical Physics, University Hospital Southampton, Southampton SO16 6YD, U.K. (email: neil.obrien@uhs.nhs.uk; robert.marchbanks@uhs.nhs.uk; tony.birch@uhs.nhs.uk)

The established clinical breathing apparatus is shown in Figs. 1 and 2. The red cap on the end has an orifice for air leakage to prevent glottis closure (as shown on the second unattached cap in Fig. 1). As it stands, this setup does not provide the participant or operator any form of assistance to track lung pressure profiles closely. A form of airflow control is needed to help assist them in their tracking ability.

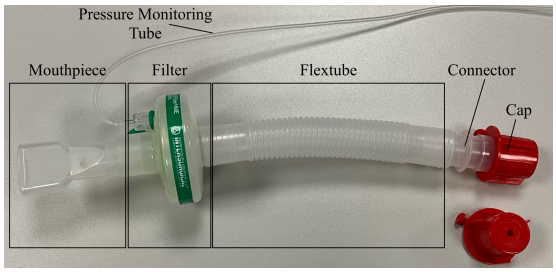

Fig. 1. Breathing tube, pressure sensor and removable cap used to measure lung pressure clinically.

Fig. 2. Current clinical setup used for lung pressure profiling.

Currently no research has investigated the application of closed loop control to airway pressure during forced exhalation. This problem is distinct from that of forced ventilation, which is used to completely replace natural respiration by controlling airflow. Key challenges include: (1) the need to react to, and interact with, the human participant's voluntary motor control system, (2) the need for an entirely passive system (air cannot be forced into a participant's lungs for safety reasons), and (3) the numerous constraints on the system.

This paper develops the first control solution to assist participants in tracking lung pressure profiles. The approach employs a setup that is suitable for clinical deployment. Since active approaches (e.g. forcing air into or out of the lungs) are unfeasible, the approach is to control airflow from the tube by adding a valve whose aperture is varied in real-time.

This research makes three novel contributions to airflow control during forced exhalation: it develops

1 - a combined time-varying model of lung dynamics, diaphragm contraction, voluntary motor control, reaction delay, and valve resistance;
2 - a model identification procedure that determines the model parameters, balancing accuracy whilst maintaining fast computation;
3 - a model-based control approach that optimises future performance by modifying valve position.

The latter is based on model predictive control (MPC), however it adjusts an internal parameter of the model (valve aperture) rather than an input signal as is conventional. It also embeds an internal valve control loop that addresses hysteresis and dead-band. Note that preliminary results appeared in [15] using a far simpler model, a restrictive identification procedure, and no experimental results.

The paper is arranged as follows: Section II develops the system model and summarises the constraints in order to yield a comprehensive problem description. Section III derives an optimal solution using the MPC framework. Sections IV and V then describe the experimental test procedure and results confirming efficacy. Conclusions are set out in Section VI.

II. Problem Description

In this section the lung pressure profile tracking problem described previously and shown in Fig. 2 is first formalised, and then a model structure and problem description are developed.

During each clinical pressure tracking experiment, the target pressure profile, $r(t)$, is displayed to the participant on a screen from time $t = 0$ up until the present time t. This screen also shows the pressure measured in the breathing tube, $P(t)$. Each test runs over the interval $t \in [0, T]$, where T is the overall duration. The target pressure is higher than ambient pressure, so the participant must always be exhaling. The only means of assisting tracking is by replacing the cap of the breathing tube (Fig. 1), by a controlled valve which uses its position, $V(t)$, to adjust airflow out of the tube. The aim of this work is to control $V(t)$ such that $P(t)$ tracks $r(t)$ as closely as possible.

A. Forced Respiration Dynamics

During natural respiration the diaphragm/intercostal muscles contract to inhale air through the trachea/bronchi and into the lungs. Gaseous exchange of oxygen and carbon dioxide occurs between the alveoli and surrounding blood vessels before the muscles relax and air is exhaled. Models of natural respiration comprise gas exchange and all the elements of human respiratory control (chemoreceptors, neuronal circuits in the brain which generate respiratory rhythm, and the respiratory muscles) [16]. However, the development of control approaches has hitherto been limited and focuses on medical ventilators, which employ far simpler models of the passive interaction between airway pressure and alveoli airflow [17]–[23]. These models represent the major compliance, resistance and inertance components as lumped parameters. An electrical analogue is typically employed where - pressure (P) $\equiv$ voltage (V); airflow (Q) $\equiv$ current; compliance (C) $\equiv$ capacitance (C); inertance (L) $\equiv$ inductance (L).

The current application differs fundamentally from those above since the aim is to assist the participant's voluntary motor control of respiration rather than replace it. Instead of using a controlled ventilation pump, the pressure must be generated by the participant themselves. To model this means the conventional lumped parameter representation of passive lung dynamics must be:

(a) extended to include a breathing tube housing a variable resistance valve;
(b) augmented by the action of diaphragm/intercostal muscles controlled by the participant's voluntary motor feedback of the tracking task;
(c) able to handle hard constraints such as maximum and minimum resistances and the pressure/volume limits imposed by forced exhalation.

Fig. 3 shows an electrical analogue model of the lungs, in which air inertance is denoted L, airway resistance R, and lung compliance C_a. This lumped parameter form has been

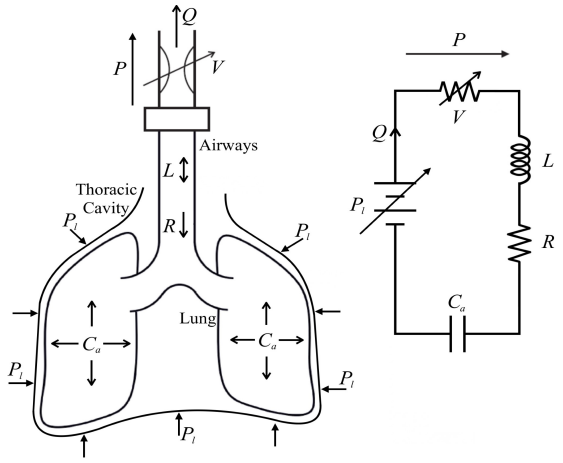

Fig. 3. Left - Lung model showing air inertance L, airway resistance R, valve resistance V and lung compliance C_a. Right - equivalent electrical analogue.

chosen due to its success for ventilator design, however in the proceeding analysis R, C_a and L can be replaced with more detailed representations of airway branching. To address point (a), variable valve resistance is included in the form of variable resistor, $V(t)$. Here laminar flow is assumed, so that the Hagen-Poiseuille equation enables valve resistance $V(t)$ to be related directly to the valve aperture (which is the controlled variable). Voltage $P(t)$ is the pressure difference (cmH_2O) measured across the valve, and corresponds to the pressure at the entrance to the participant's airway. The airflow rate out of the lungs/tube corresponds to the current $Q(t)$.

To incorporate point (b), the pressure source signal $P_l(t)$ has been added to represent the effect of respiratory muscle movement (cmH_2O) under the participant's voluntary control (i.e. the pressure in the lungs). To determine how $P_l(t)$ is generated, there are a variety of models of voluntary human sensorimotor control available (see, e.g. [24]), and the most general form comprises a feedback component, together with a feed-forward predictive planning component. Combining this form with the above model yields the overall airway tracking system shown in Fig. 4. Here operator G comprises the respiratory tract and breathing apparatus depicted in Fig. 3, the diaphragm/intercostal muscle control dynamics are represented by operator K, and the motor control return loop feedback by operator H. The feed-forward planning component is denoted by operator F, and the pressure reference is $r(t)$.

To address point (c) it is necessary to specify several constraints: Limits on the maximum airway pressure, $P(t)$,

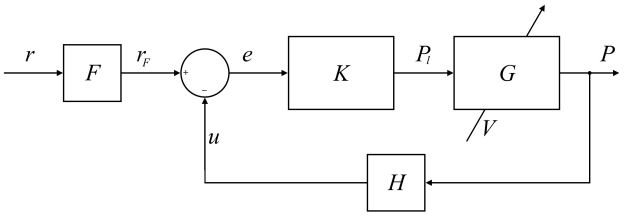

Fig. 4. Voluntary pressure reference tracking system with valve resistance V.

and the total exhaled volume (vital capacity) $\int_{t=0}^{T} Q(t)$ are necessary to ensure that the participant does not overexert themselves during pressure profiling. A maximum resistance V_{max} ensures the glottis can remain open throughout measurement, and a minimum resistance V_{min} is a physical apparatus limitation. A minimum profile length of $T = 20$ seconds aligns with TMD measurement profiles.

The overall system description can now be stated:

Definition 1 (System Description): The assistive pressure tracking system takes the form of Fig. 4 where operators K and H model voluntary sensorimotor control of the diaphragm and intercostal muscles with LTI discrete time dynamics represented by the state-space quadruples (A_K, B_K, C_K, D_K) and (A_H, B_H, C_H, D_H) respectively. Operator F models the feed-forward, predictive component of sensorimotor control by the state-space quadruple (A_F, B_F, C_F, D_F). The assisted respiration dynamics G, $(P_l, V) \mapsto P$ are shown in Fig. 3, where valve resistance V is a controlled parameter. The dynamics of G can be represented by the LTV continuous time state-space system

$$\dot{x}_G(t) = \underbrace{\begin{bmatrix} 0 & \frac{1}{C_a} \\ -\frac{1}{L} & -\frac{(R+V(t))}{L} \end{bmatrix}}_{A_G(V(t))} x_G(t) + \underbrace{\begin{bmatrix} 0 \\ -\frac{1}{L} \end{bmatrix}}_{B_G} \begin{bmatrix} P_l(t) \\ V(t) \end{bmatrix},$$
$$P(t) = \underbrace{[0 \;\; V(t)]}_{C_G(V(t))} x_G(t), \qquad t \in [0, T] \tag{1}$$

so that discretisation with sample period T_s yields the discrete time state-space system

$$x_{G,k+1} = \underbrace{e^{A_G(V_k)T_s}}_{A_G(V_k)} x_{G,k} + \underbrace{(e^{A_G(V_k)T_s} - I)B_G A_G^{-1}(V_k)}_{B_G(V_k)} \begin{bmatrix} P_{l,k} \\ V_k \end{bmatrix}$$
$$P_k = \underbrace{[0 \;\; V_k]}_{C_G(V_k)} x_{G,k}, \qquad k = 1, \cdots, N \tag{2}$$

where subscript k denotes the sample number, i.e. $V_k = V(kT_s)$ and $N = T/T_s$. The composite G and K dynamics $e \mapsto y$ can then be written as the discrete time state-space triple $(A_{KG}(V_k), B_{KG}(V_k), C_{KG}(V_k))$ where

$$A_{KG}(V_k) = \begin{bmatrix} A_K & 0 \\ B_G(V_k)C_K & A_G(V_k) \end{bmatrix}, \tag{3}$$
$$B_{KG}(V_k) = \begin{bmatrix} B_K \\ B_G(V_k)D_K \end{bmatrix}, \; C_{KG}(V_k) = \begin{bmatrix} 0 & C_G(V_k) \end{bmatrix}$$

which then enable the closed loop system $r_F \mapsto P$ to be represented as the state-space triple $A_{cl}(V_k) =$

$$\begin{bmatrix} A_{KG}(V_k) - B_{KG}(V_k)D_H C_{KG}(V_k), & -B_{KG}(V_k)C_H \\ B_H C_{KG}(V_k) & A_H \end{bmatrix}$$
$$B_{cl}(V_k) = \begin{bmatrix} B_{KG}(V_k) \\ 0 \end{bmatrix},\ C_{cl}(V_k) = \begin{bmatrix} C_{KG}(V_k) & 0 \end{bmatrix} \tag{4}$$

Incorporating F then means the overall system $r \mapsto P$ can be represented by the system

$$x_{k+1} = \underbrace{\begin{bmatrix} A_F & 0 \\ B_{cl}(V_k)C_F & A_{cl}(V_k) \end{bmatrix}}_{A(V_k)} x_k + \underbrace{\begin{bmatrix} B_F \\ B_{cl}(V_k)D_F \end{bmatrix}}_{B(V_k)} r_k$$
$$P_k = \underbrace{\begin{bmatrix} 0 & C_{cl}(V_k) \end{bmatrix}}_{C(V_k)} x_k, \qquad k = 1, \cdots, N, \qquad x_0 = 0 \tag{5}$$

Having defined the voluntary pressure reference tracking system dynamics, the control problem can now be stated.

Definition 2 (Valve Assistance Problem): Consider the system shown in Fig. 4 with discrete state-space matrices (5) running over samples $k = 1, 2, \cdots, N$. The control problem is to select the sequence of valve resistance values $\bar{V} = (V_1, V_2, \cdots, V_N)$ such that the error 2-norm is minimised, i.e.

$$\arg\min J(\bar{V}), \quad J(\bar{V}) := \sum_{i=1}^{N} (r_i - P_i)^2. \tag{6}$$

subject to dynamics (5) and constraints

$$0 \le P_k \le P_{max}, \tag{7a}$$
$$V_{min} \le V_k \le V_{max}, \qquad k = 1, \cdots, N \tag{7b}$$
$$\sum_{k=0}^{N} Q_k \le vc \tag{7c}$$
$$N = T/T_s, \quad T \ge 20 \text{ seconds} \tag{7d}$$

where Q_k is the airflow at time step k, given by $Q_k = P_k/V_k$ and vc is the vital capacity.

The Valve Assistance Problem is fundamentally different to a conventional control problem since it involves changing a parameter within the plant dynamics (i.e. the valve resistance V_k) on every sample, rather than a control signal input. To select an appropriate approach, control structures used in existing respiratory applications are reviewed in Section III.

B. Identification

The system parameters within (1)-(5) must be identified using a test procedure suitable for clinical application. Preliminary research solved this problem for a restrictive form of external disturbance [15], however a general procedure is now proposed that removes assumptions on the system disturbances.

Definition 3 (Identification Problem): Consider the time-varying discrete closed loop system shown in Fig. 4 with components (1)-(5). Given a set of sampled experimental input-output data $\{\tilde{r}_i, \tilde{P}_i\}_{i=1,\cdots,N}$, and corresponding valve resistance sequence $\tilde{V} = (\tilde{V}_1, \tilde{V}_2, \cdots, \tilde{V}_N)$, the identification problem is to compute the parameter vector $\hat{\theta}$ containing all the unknown parameters within K, G, and H. This corresponds to the minimisation problem

$$\min_{\hat{\theta}} \sum_{k=1}^{N} (\tilde{P}_k - P_k)^2 \tag{8}$$

where θ contains all unknown coefficients of F, K, G, and H, subject to dynamics (1)-(5) with input $\tilde{r}$ and valve sequence vector $\tilde{V}$.

III. Model Predictive Valve Control (MPVC)

Controllers for respiration have focused on medical ventilation, where they replace natural breathing. This means they neglect voluntary muscle and motor control processes, and their aim is solely to adjust flow rates and pressures to supply adequate gas exchange in a physiologically safe manner and in the presence of system constraints. In particular, proportional, integral and derivative (PID) control has provided a rapid response, but lacks accuracy [19], [21], [25]. Fuzzy adaptive algorithms [21] and iterative learning control [25] have both been implemented in conjunction with PID for medical ventilation to improve performance. Machine learning has been used to set ventilator categories based on patient conditions, however it requires substantial data and training [26]. MPC was applied to medical ventilation in [16], where it adjusted the minute volume ventilation to track a minute volume reference. It handled hard constraints on minute volume while still providing close to optimal support for patient breathing activity.

The above controllers cannot be directly applied to the Valve Assistance Problem (*Definition 2*) directly since it does not take a typical structure. However, they motivate applying MPC in an alternative form. The fact that this is a parameter time-varying varying problem does not pose undue difficulty, as the system can be reformulated in a straightforward manner. MPC operates by dividing the measurement period, N, into smaller predictive horizons in order to reduce computation. However, here the maximum volume constraint (7c) affects the entire measurement period, meaning that the finite horizon solution may be highly non-optimal (e.g. causing the participant to quickly run out of breath). To ensure an excessive flow is not exhaled at an early stage, this constraint will be implemented by adding a term to the cost to encourage conservation of breath. To reduce computational load, the set of valve resistances will also be reduced to a discrete set, $\mathcal{V}$. This gives rise to the following solution:

Definition 4 (Model Predictive Valve Control (MPVC)): The Valve Assistance Problem (6) with constraints (7) is solved by computing the sequence of valve resistances $\bar{V} = (V_1, V_2, \cdots, V_N)$ that minimise finite horizon cost function

$$\arg\min J(\bar{V}),\ J(\bar{V}) := \sum_{i=1}^{N} (r_i - P_i)^2 \Phi_i + (V_{max} - V_i)^2 \Psi_i \tag{9}$$

where Φ_i and Ψ_i are positive definite and semi-definite weights respectively. This is subject to dynamics (1)-(5), and

the constraint that V_i is taken from a set of pre-defined valve resistances, i.e.

$$V_i \in \mathcal{V}, \quad \mathcal{V} = \{v_1, , v_2, \cdots, v_n\}, \quad V_{min} \leq v_i \leq V_{max}, \tag{10}$$

and the remaining constraint (7a).

To solve (9), MPVC replaces it with the receding horizon approximation (i.e. stage cost)

$$\arg\min J(\bar{V}_k),\ J(\bar{V}_k) := \sum_{i=k}^{k+m} (r_i - P_i)^2 \Phi_i + (V_{max} - V_i)^2 \Psi_i \tag{11}$$

subject to dynamics (1)-(5) and constraints (7a), (10). This is computed at each sample k. Here m is the prediction horizon, and the stage valve resistance sequence on sample k is $\bar{V}_k = (V_k, V_{k+1}, \cdots, V_{k+m})$. The first element of $\bar{V}_k$ is then applied: $V_k = [1\ 0\ \cdots\ 0]\bar{V}_k$. The overall MPVC system is shown in Fig. 5.

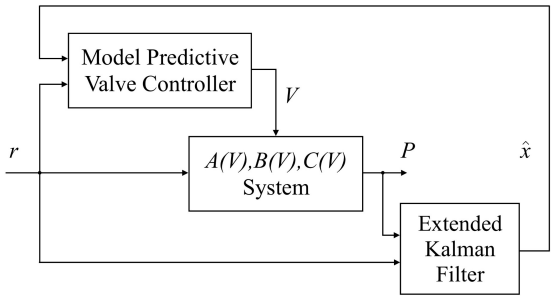

Fig. 5. Block diagram of the MPVC system where r is the pressure profile input and $\hat{x}$ is the estimated plant state.

Computing cost function (11) requires the current state x_k within system (5). This is not measurable, but an approximation, $\hat{x}_k$, can be computed using the time-varying Extended Kalman Filter system [27], given by

$$\begin{aligned} M_k &= S_k C^\top(V_k)(C(V_k)S_k C^\top(V_k) + \lambda_m)^{-1}, \\ \hat{x}_k &= \hat{x}_k + M_k(y_k - C(V_k)\hat{x}_k), \\ S_k &= (I - M_k C(V_k))S_k, \\ \hat{x}_{k+1} &= A(V_k)\hat{x}_k + B(V_k)r_k, \\ S_{k+1} &= A(V_k)S_k A^\top(V_k) + B(V_k)\mu_p B^\top(V_k), \end{aligned} \tag{12}$$

with initial values $\hat{x}_0 = 0$ and $S_0 = B_{V_{max}}\mu_p B_{V_{max}}^\top$. Here M_k is the Kalman gain matrix, S_k is the state error covariance matrix, λ_m is the measurement noise covariance matrix, and μ_p is the process noise covariance matrix.

Solving (11), subject to (5), (7) and $V_k \in \mathcal{V}$, on each sample k is a non-convex problem and can be addressed using an exhaustive search or via specialist solvers such as non-linear or integer programming.

To apply these solvers, note that cost (11) can be written in matrix form as

$$\begin{aligned} J(\bar{V}_k) = (\vec{r}_k - \vec{P}_k)^\top \bar{\Phi}(\vec{r}_k - \vec{P}_k) \\ + (V_{max} - \bar{V}_k)^\top \bar{\Psi}(V_{max} - \bar{V}_k) \end{aligned}$$

where $\vec{r}_k = [r_k, r_{k+1}, \cdots, r_{k+m}]^\top$, $\vec{P}_k = [P_k, P_{k+1}, \cdots, P_{k+m}]^\top$, $\bar{V}_{max} = [V_{max}, \cdots, V_{max}]^\top$, $\bar{\Phi} = \text{diag}\{\Phi, \cdots, \Phi\}$, $\bar{\Psi} = \text{diag}\{\Psi, \cdots, \Psi\}$, and

$$\vec{P}_k = \Gamma(\bar{V}_k)\vec{r}_k + \Xi(\bar{V}_k)\hat{x}_k \tag{13}$$

with

$$\Gamma(\bar{V}_k) = \begin{bmatrix} 0 & 0 & \cdots & 0 & 0 \\ \gamma(1,0) & 0 & \cdots & 0 & 0 \\ \gamma(2,0) & \gamma(2,1) & \cdots & 0 & 0 \\ \vdots & \vdots & \ddots & \vdots & \vdots \\ \gamma(m,0) & \gamma(m,1) & \cdots & \gamma(m,m-1) & 0 \end{bmatrix}$$

$$\Xi(\bar{V}_k) = [\xi(0), \xi(1), \cdots, \xi(m)]^\top$$

where

$$\gamma(a,b) := C(V_{k+a})A(V_{k+a-1}) \times \cdots \times A(V_{k+b+1})B(V_{k+b})$$

and

$$\xi(a) := C(V_{k+a})A(V_{k+a-1}) \cdots A(V_k).$$

A. Comparative Control Methods

MPVC provides a highly accurate solution to the Valve Assistance Problem (*Definition 2*), however simpler methods may also provide potential solutions. Based on the review in Section III, traditional controllers cannot be directly applied to this parameter control problem, since the controller is adjusting an internal parameter of the system (V) rather than an input signal. However, they motivate simple structure approaches such as PID. To establish its applicability, consider the dynamics shown in Fig. 3

$$P_l(t) = L\frac{dQ(t)}{dt} + (R + V(t))Q(t) + \frac{1}{C_a}\int Q(t), \tag{14}$$

$$P(t) = Q(t)V(t) \tag{15}$$

which, assuming the rate of change of airflow is small, simplify to

$$P_l(t) - \frac{1}{C_a}\int Q(t) = RP(t)/V(t) + P(t) \tag{16}$$

$$\Rightarrow P(t) = \frac{aV(t)}{R + V(t)} \tag{17}$$

around an operating point $a = P_l - \frac{1}{C_a}\int Q(t)$. Since a and R are positive, the dynamics $V(t) \mapsto P(t)$ comprise a smooth, monotonically increasing function that passes through $(0,0)$, with an amplitude that depends on the flow volume. This monotone relationship suggests that a PID type control action would effectively reduce the error $e_k = r_k - P_k$. This motivates implementing a proportional controller of the form

$$V_k = V_{e_0} - K_{p_e} e_k \tag{18}$$

where V_{e_0} is a resistance offset that moves the system to a pressure operating point concurrent to the r operating point. K_{p_e} is set such that constraint (7b) is adhered to. A drawback to proportional control is possible valve resistance oscillation due to rapid pressure changes. Large pressure drops may also cause a significant drop in valve resistance creating a high airflow, causing the participant to run out of air in their

lungs more quickly. These issues can be addressed using integral control, which amalgamates valve resistance over time depending on error e_k, taking the form

$$V_k = V_{e_0} - K_{i_e} \sum_{i=k_{ec}}^{k} e_i \tag{19}$$

with limits V_{min} and V_{max}. Here K_{i_e} is the integral coefficient of the error and k_{ec} is the time when the error most recently changed sign.

B. Valve Control System

In the preceding sections it has been assumed that the valve resistance, V_k, can be directly set at each time instant k by the controller. However, in reality, the controlled variable is a pulse-width modulation (PWM) duty cycle sent to the valve, which affects the airflow through the valve (thus the valve resistance) in the following indirect manner:

- The PWM signal, ρ, dictates the magnitude of a proportional current (gain κ) that is applied to the valve;
- the resultant current, $\kappa\rho$, changes the flow coefficient, K_v, of the valve by actuating the valve position. These two variables are related by a static nonlinear function, $K_v = \eta(\kappa\rho)$, which includes hysteresis;
- The value of K_v relates the pressure and flow via $K_v = Q/\sqrt{P}$.

A resistance-tuning controller is therefore needed to continually adjust the PWM duty cycle signal ρ such that the required valve resistance, V_k, is achieved. This is done by measuring the pressure value P_k, and computing the necessary flow rate, denoted $Q_{r,k}$, that achieves V_k at every sample. Then a proportional control loop (gain K_ρ) is applied to force Q_k to track this $Q_{r,k}$. The resulting controller is shown in Fig. 6.

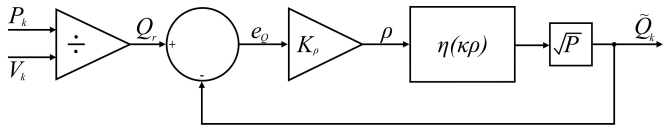

Fig. 6. Block diagram of the resistance-tuning controller

IV. Experimental Application

Fig. 7 shows the experimental setup. Compared to the standard clinical setup shown in Fig. 1, the flextube has been removed to reduce compliance (which is assumed zero in the model). The modified system shown in Fig. 7 has retained the mouthpiece, filter and pressure monitoring tube as in Figs. 1 and 2. An airflow sensor (*Sensirion SFM3020 series*) is added to enable accurate resistance calculations and a variable PWM valve (*Burkert 6024 series (12mm)*) is added to control airflow resistance. The pressure sensor is a *Panasonic PS-A series (6KPa)*. The measurement hardware and software are *National Instruments myRIO-1900 series* and *Labview 2019* respectively. All identification, control design, and analysis computations were performed in *MATLAB R2020b*.

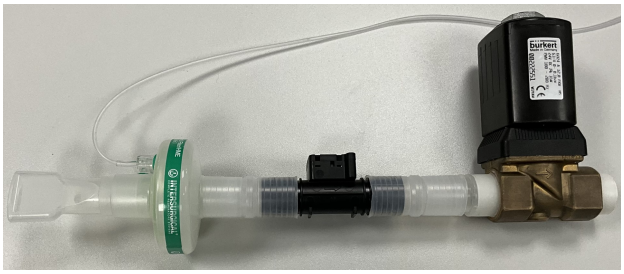

Fig. 7. Breathing tube, pressure sensor, airflow sensor and variable valve used to measure lung pressure

A. Procedure

During testing, all participants were seated in an upright position and used the same equipment (apart from different mouthpieces and filters) in a standardised position. Prior to testing, the pressure and airflow sensors were calibrated by placing them on a flat surface as shown in Fig. 7 and applying an offset to produce zero readings.

B. Model Structure Selection

Since the tracking task is reactive (i.e. the pressure reference is shown to the participant and they are required to immediately attain it), the planning component F is set equal to a perception delay of 0.2s, corresponding to the average human response time to a sensory stimulus [28]. Based on established models of human motor control [24] K and H are chosen to realise a proportional-integral feedback controller (respective gains K_p and K_i). An additional delay is incorporated into K to account for the decision delay of 0.1s. This selection leads to the forms:

$$A_F = \begin{bmatrix} 0 & 0 & \cdots & & 0 \\ 1 & 0 & \ddots & \ddots & \vdots \\ 0 & 1 & \ddots & \ddots & \vdots \\ \vdots & \ddots & \ddots & \ddots & \vdots \\ 0 & \cdots & 0 & 1 & 0 \end{bmatrix}, \quad B_F = \begin{bmatrix} 1 \\ 0 \\ 0 \\ \vdots \\ 0 \end{bmatrix},$$
$$C_F = \begin{bmatrix} 0 & 0 & 0 & \cdots & 1 \end{bmatrix} \tag{20}$$

and

$$A_K = \begin{bmatrix} 0 & 0 & \cdots & & 0 & 0 \\ 1 & 0 & \ddots & \ddots & \vdots & \vdots \\ 0 & 1 & \ddots & \ddots & \vdots & \vdots \\ \vdots & \ddots & \ddots & \ddots & \vdots & \vdots \\ 0 & \cdots & 0 & 1 & 0 & \vdots \\ 0 & \cdots & \cdots & \cdots & T_s & 1 \end{bmatrix}, \; B_K = \begin{bmatrix} 1 \\ 0 \\ 0 \\ \vdots \\ 0 \end{bmatrix},$$
$$C_K = \begin{bmatrix} 0 & \cdots & 0 & K_p & K_i \end{bmatrix}. \tag{21}$$

Accepted values of L fall between 0.001 and 0.01 and have negligible effect on the tracking response thus will be omitted from the G dynamics.

Therefore the overall closed loop dynamics are given by state-space system (5) with

$$A(V_k) = \begin{bmatrix} 0 & 0 & \cdots & \cdots & \cdots & 0 & \frac{-V_k}{R+V_k} \\ 1 & 0 & \ddots & \ddots & \ddots & \ddots & 0 \\ 0 & 1 & \ddots & \ddots & \ddots & \ddots & \vdots \\ \vdots & \ddots & \ddots & \ddots & \ddots & \ddots & \vdots \\ \vdots & \cdots & 0 & 1 & 0 & \ddots & \vdots \\ \vdots & \cdots & \cdots & 0 & T_s & 1 & 0 \\ 0 & \cdots & \cdots & 0 & K_pT_s & K_iT_s & exp\left(\frac{-T_s}{(R+V_k)C_a}\right) \end{bmatrix}$$
$$B(V_k) = \begin{bmatrix} 1 & 0 & \cdots & 0 \end{bmatrix}^\top, C(V_k) = \begin{bmatrix} 0 & \cdots & 0 & \frac{V_k}{R+V_k} \end{bmatrix} \tag{22}$$

Lung compliance, C_a is set to 0.1 L/cmH_2O as this value accurately fits all subjects [22]. The search parameter vector within (8) therefore becomes $\hat{\theta} = (R, K_p, K_i)$.

C. Identification Data Collection

The next step is to capture the dynamics of the system using the identification procedure in Section II-B. This requires that the pressure sequences $\{\tilde{r}_i\}_{i=1,\cdots,N}$ and corresponding valve resistance sequences $\{\tilde{V}\}_{i=1,\cdots,N}$ are sufficiently exciting while minimal in number to be practically feasible.

This data set was constructed by amalgamating 24 separate identification tests, each lasting at least 2 seconds. The first set of 12 tests captured the participant's response to a step reduction in valve resistance, while they attempted to track a constant reference pressure. The reference value r_{id}, was taken from the set $\{10, 20, 30\}$ with units cmH_2O. The valve was initially closed ($V = \infty$), and the participant was required to reach the required value of r_{id}. Then the valve opened to a specified resistance V_{id} taken from the set $\{20, 40, 60, 80\}$ with units cmH_2O/L/s. Measurements began and the participant was required to get the pressure back up to r_{id} as quickly as possible (see Fig. 10).

The second set of 12 tests captured the participant's response to a step increase in pressure, starting at a pressure of $P = 0$ cmH_2O. Once the valve opened, they had to reach the reference pressure r_{id} as quickly as possible and settle (see Fig. 11). The tests were performed with the same combination of references (r_{id}) and resistances (V_{id}) as the first procedure.

The 24 sets of data were then grouped according to the valve resistance applied and the test. This produced eight groups (two tests types, four resistance values of V_{id} each). For each test and resistance level (i.e. eight groups mentioned above) the data were normalised over the three reference pressures and an average was taken. This produced eight data sets which are used for identification purposes.

This normalisation is possible since the same change in V_k occurs at each pressure reference r, the dynamics (22) remain the same thus superposition applies. Therefore the output can be scaled by dividing by the pressure reference level. Taking an average of each of the eight groups reduces the number of sets used to compare against during identification.

The eight averaged data sets were combined to form the overall sets $\{\tilde{r}_i, \tilde{P}_i\}_{i=1,\cdots,N}$, $\{\tilde{V}\}_{i=1,\cdots,N}$. Then cost function (8) was minimised over the search space of suitable parameters

$$\hat{\theta} \in \{(R, K_p, K_i) \mid R \in \{1, 2, \cdots, 20\}, K_p \in \{1, 2, \cdots, 20\}, K_i \in \{0, 1, \cdots, 20\}\}. \tag{23}$$

To assess how closely the resulting model fitted a measured data set $\{\tilde{r}, \tilde{P}, \tilde{V}\}$, the percentage accuracy was computed as

$$\left(1 - \frac{\sum_{i=1}^{N}(\tilde{P}_i - P_i)^2}{\sum_{i=1}^{N}\tilde{P}_i^2}\right) \times 100 \tag{24}$$

where $\tilde{P}$ is the measured pressure, and P is the output of model (1)-(5) with input $\{\tilde{r}, \tilde{V}\}$. This will be termed the *fitting accuracy* when using identification data, and *prediction accuracy* when using any other data.

D. Control Application

The pressure and airflow sampling frequency was set at 100Hz ($T_s = 0.01$s) to match that of clinical TMD measurements. Additionally, the valve regulator in Section III-B also operated at 100Hz. In order for the control schemes to be viable for use on low-cost hardware with the potential for mass screening, the control cycle frequency was limited to 10Hz ($T_c = 0.1s$). The prediction horizon for MPVC was similarly limited to $m = 5$, i.e. the controller predicts the model output up to 0.5 seconds ahead of the current time instance. The number of possible valve resistance values was limited to three to ensure computations were completed within the sampling time.

Based on preliminary testing, the selected valve resistance values were determined to comprise: a maximum value of resistance which does not allow glottal closure, a value to assist the participant in decreasing lung pressure, and a value to release pressure. This resulted in the permissible set of valve resistances $\mathcal{V} := \{80, 160, 1000\}$. Solving the non-convex MPVC problem (11) was then achieved by evaluating the stage cost J for all $|\mathcal{V}|^m$ possible valve resistance sequences. The controller then selects the lowest stage cost and applies the first element of solution $\bar{V}_k$.

Five control schemes were tested with each participant. The first approach employed a constant valve resistance. This replicates the resistance of the red cap in Fig. 1, and is therefore the standard experimental approach. This is the baseline approach to lung pressure profile tracking.

The second approach was the discrete integral controller presented in Section III-A. This took the form (19) but the gains V_{e_0} and K_{i_e} were adapted such that

$$V_k = \begin{cases} V_{k-1} - 20, & e_k < -2, \\ 160, & -2 \leq e_k \leq 2, \\ V_{k-1} + 20, & e_k > 2. \end{cases}$$

The third approach was the discrete proportional controller (18), whose gains V_{e_0} and K_{p_e} were adapted such that

$$V_k = \begin{cases} 20, & e_k \leq -10, \\ 40, & -10 < e_k \leq -8, \\ 60, & -8 < e_k \leq -5, \\ 80, & -5 < e_k \leq -3, \\ 160, & -3 < e_k \leq 5, \\ 300, & 5 < e_k \leq 10, \\ 1000, & e_k > 10. \end{cases}$$

The choice of gains effectively limits the control action to prevent valve oscillation or high airflow.

The fourth and fifth approaches use MPVC with different Kalman Filter covariance scalar parameters, λ_m and μ_p within (12). As the ratio μ_p/λ_m increases, the process noise assumes more variance compared to the measurement noise. This has the effect of placing more reliance on the measurement data compared to the model in computing the estimated state. Modifying the ratio has a significant effect on the overall control action. Both MPVC control approaches used a covariance of $\lambda = 1$. However, the fourth and fifth control approaches use $\mu_p = 0.1$ and $\mu_p = 1$ respectively.

E. Pressure Profiles

Participants were required to perform 30 pressure tracking tests in total. These comprised six pressure profiles (cmH_2O), each repeated five times (each with a different controller). The six profiles were each composed of steps. Each step size was a multiple of a fixed amplitude Δr, and had a duration of 3 seconds. The profile had to be constrained within an overall pressure range. The parameters used to construct each profile type are as follows:

a) $10 \leq r \leq 30$, $\Delta r = 5$
b) $10 \leq r \leq 30$, $\Delta r = 10$
c) $10 \leq r \leq 40$, $\Delta r = 5$
d) $10 \leq r \leq 40$, $\Delta r = 10$
e) $10 \leq r \leq 50$, $\Delta r = 5$
f) $10 \leq r \leq 50$, $\Delta r = 10$

The step sizes were randomised so that participants could not predict them. Similarly, the order of the controllers was randomised to provide an unbiased assessment of the ability of each. Fig. 8 shows an example of a participant's response to a pressure profile.

Two safety protocols were employed to identify the lung vital capacity and pressure constraints in (7). The vital capacity was measured for each participant 3 times and an average was taken. The limit v_c was then set around 1 litre less than their vital capacity. The experiment was stopped immediately this limit was reached. Participants were also asked to exhale until they reached a maximum pressure they felt was exerting but still comfortable. Eight of the ten participants were comfortable generating a pressure above 50 cmH_2O, the other two participants generated maximums of 40 and 45 cmH_2O. In these cases the pressure profile ranges were 5-25, 10-30, and 5-35 cmH_2O and 10-30, 5-35, and 10-40 cmH_2O respectively.

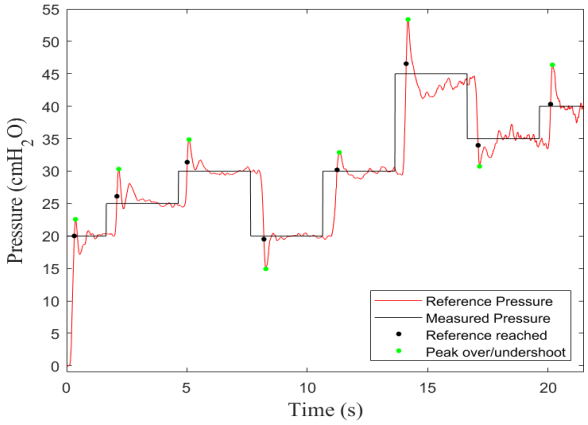

Fig. 8. Example tracking response (profile type (e)) with constant valve resistance. Black points represent the first point where the reference has been reached after a step change. Green points represent peak overshoot/undershoot.

V. Results

Following University of Southampton ethics approval (ERGO/FPSE/62619), 10 healthy participants (7 men and 3 women, age range 20-56) with no underlying health conditions were recruited onto this study. The participants will be referred to as P1-P10.

A. Model Identification

Each participant completed the identification and control tests described in Section IV. Figs. 10 and 11 show an example of the measured tracking responses and the model tracking responses for the two types of identification test.

Fig. 9 presents the model identification results in the form of box and whisker plots showing the data fitting accuracy for each participant. Three measures of model fitting accuracy (MFA) are shown:

MFA1: Fitting accuracy of the model to the averaged identification data (8 data sets, 2 second measurement period, see Section IV-C)
MFA2: Prediction accuracy of the model to all identification data (24 data sets, 2 second measurement period)
MFA3: Prediction accuracy of the model to all control data (30 data sets, 10-50 second measurement period)

For MFA1, the average of the medians, means, and IQRs over all participants are 92.3%, 91.8%, and 4.0% respectively. This shows that the participants had good consistency after a short practice period, it also shows that the model and identification process is effective for practical use. MFA1 is highest as these data were used to identify the model.

For MFA2, the combined average of the medians, means and IQRs over all participants are 87.6%, 87.0% and 6.8% respectively. This not only shows that the model is accurate but also that the participants are relatively consistent in their pressure reference tracking and response to specific resistance changes.

MFA3 measures the model accuracy during the participants' controlled tracking results. Fig. 12 shows the same data as in Fig. 8 but with the predicted output of the identified model

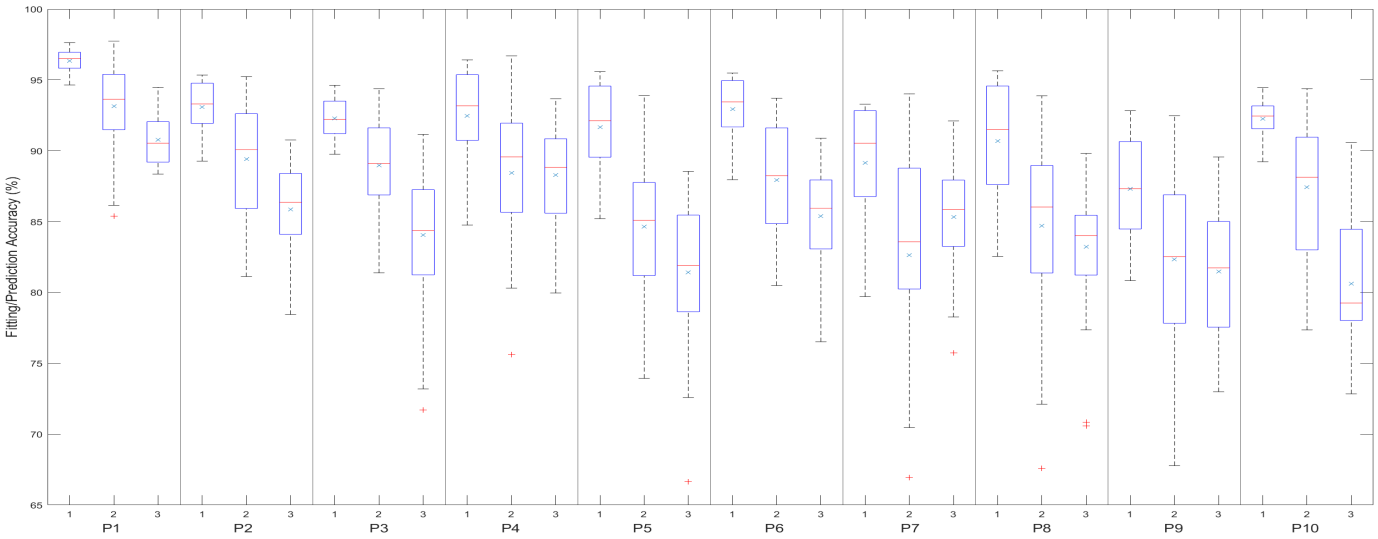

Fig. 9. Box and whisker plots of model fitting and prediction accuracies of identification and control data corresponding to each participant. Columns labelled: 1 represent MFA1; 2 represent MFA2; 3 represent MFA3. The central line of the boxes represents the median and the 'x' mark represents the mean.

TABLE I
TABLE OF MEDIANS AND MEANS FROM THE METRICS IN FIGS. 14-18

Control Method	**Combined Statistical Data**									
	Average Airflow (L/s)		**2-error norm**		**Fall Time (s)**		**Rise/Fall 2-error norm**		**Abs. Prop. Over/undershoot**	
	Median	Mean	Median	Mean	Median	Mean	Median	Mean	Median	Mean
Constant Resistance	0.1307	0.1378	0.2730	0.2677	0.6600	0.7301	0.3791	0.5155	0.2285	0.3596
Proportional-Integral	0.0988	0.1007	0.2647	0.2681	0.6400	0.6620	0.3999	0.5364	0.2340	0.3765
Proportional	0.1488	0.1543	0.2347	0.2395	0.5500	0.6204	0.3355	0.4378	0.2400	0.3445
MPVC 1	0.0471	0.0498	0.2130	0.2260	0.5200	0.5660	0.3115	0.4277	0.1935	0.3073
MPVC 2	0.0495	0.0512	0.2251	0.2259	0.5600	0.6088	0.3168	0.4309	0.1780	0.2729

TABLE II
TABLE OF RANGES AND NUMBER OF DATA POINTS, WITH OUTLIERS IN BRACKETS, FROM THE METRICS IN FIGS. 14-18

Control Method	**Combined Statistical Data**				
	Average Airflow (L/s)	**error 2-norm**	**Fall Time (s)**	**Rise/Fall 2-error norm**	**Abs. Prop. Over/undershoot**
	Range				
Constant Resistance	0.0530-0.2368	0.1320-0.4641	0-2.55	0.0110-3.0386	0-2.3860
Proportional-Integral	0.0339-0.2189	0.1656-0.4206	0-2.63	0.0106-3.1497	0.0003-4.9780
Proportional	0.0656-0.2886	0.1351-0.3607	0-2.55	0.0020-1.4428	0.0023-2.5640
MPVC 1	0.0176-0.1026	0.1466-0.3636	0-1.71	0.0081-3.2357	0-2.5720
MPVC 2	0.0172-0.0838	0.1089-0.3435	0-1.87	0.0022-2.2928	0.0015-3.3800
	Number of Data Points				
Constant Resistance	60(0)	60(3)	151(15)	422(18)	422(24)
Proportional-Integral	60(0)	60(0)	187(16)	461(21)	461(30)
Proportional	60(2)	60(0)	143(13)	384(11)	384(17)
MPVC 1	60(1)	60(0)	200(11)	506(23)	506(27)
MPVC 2	60(0)	60(0)	197(14)	517(25)	517(31)

overlaid in blue. The combined average of the medians, means and IQRs over all participants are 84.9%, 84.6% and 5.3% respectively. This further confirms the validity of the model and identification procedure.

B. Control

The following metrics were computed for each profile tracking test: average airflow; 2-norm of profile tracking error; time taken to reach the profile pressure after a step down (labelled 'fall time'); 2-norm of profile tracking error after a step up or step down; absolute value of overshoot/undershoot to a step change in proportion to the magnitude of the step change. These metrics are defined in more detail below.

Figs. 14 - 18 show box and whisker plots of each metric. Each box and whisker corresponds to the pooled data from all participants for a particular control type and is labelled on the plots as follows:

1) Constant valve resistance
2) Proportional-integral (PI)
3) Proportional
4) MPVC with Kalman parameters $\lambda_m = 1$, $\mu_p = 0.1$
5) MPVC with Kalman parameters $\lambda_m = 1$, $\mu_p = 1$.

As previously described, Control Type 1 (constant valve resis-

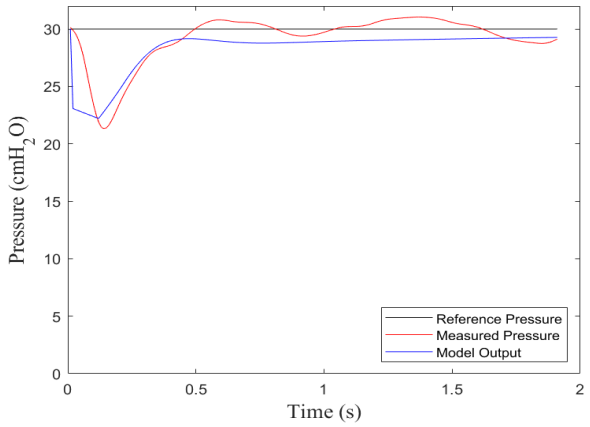

Fig. 10. Sample tracking response of first identification procedure ($r_{id} = 30$, $V_{id} = 20$)

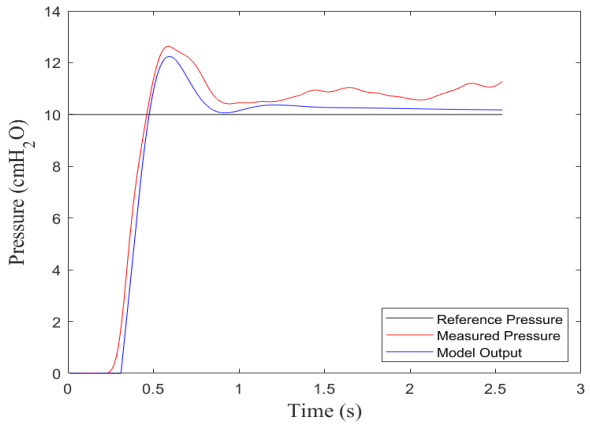

Fig. 11. Sample tracking response of second identification procedure ($r_{id} = 10$, $V_{id} = 60$)

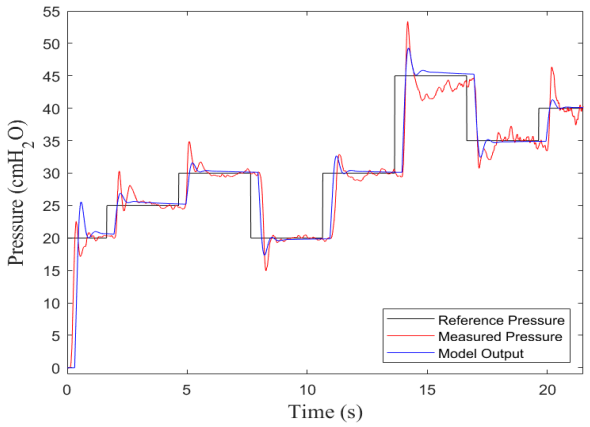

Fig. 12. Sample tracking response with constant valve resistance (Fig. 8, profile type (e)) with predicted model output overlaid

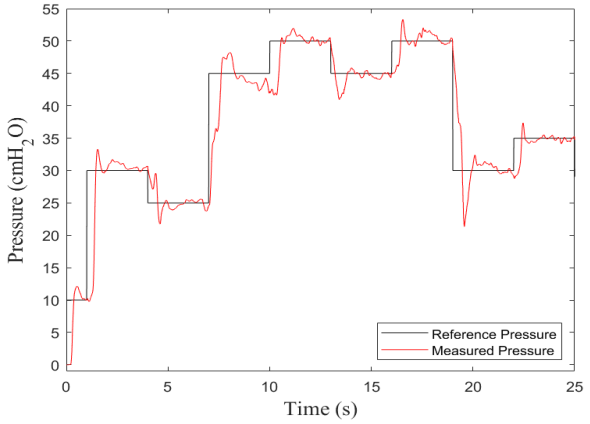

Fig. 13. Sample tracking response with MPVC assistance (profile type (e))

tance) is the baseline approach against which Control Types 2-5 are compared below.

Table I shows the medians and means and Table II presents the ranges and number of data points from Figs. 14-18. In Table I, the highlighted values are the most desirable values.

To ensure the vital capacity constraint (7c) and time constraint (7d) are both met, average airflow must be less than 0.15 L/s (assuming a minimum vital capacity of 3 litres). PI control shows a small reduction in airflow, proportional control shows a slight increase and both MPVC approaches show a significant decrease as well as a smaller range. Lower average airflow corresponds to longer measurement periods, therefore MPVC is the best approach for this metric, providing a 64% decrease in average airflow.

The 2-norm of the tracking error indicates how well the participants track the profile; the lower the 2-norm, the better the tracking. PI control shows similar levels of tracking error to the constant valve resistance case, but both proportional and MPVC show a reduction in tracking error with the greatest reduction of 22% shown in MPVC 1.

Fall time refers to the time it takes for a participant to reach the new pressure reference value after a step-down change (e.g. black points in Fig. 8). PI control shows a similar fall time to constant valve resistance, proportional and MPVC 2 show a significant decrease by about 0.1s, while MPVC 1 shows the biggest improvement with a decrease of 0.15s (22% reduction).

The 2-norm of the rise/fall error refers to the 2-norm tracking error in the time window between a step change in reference and when the pressure reference is reached (i.e. same time window as rise/fall time). PI control shows an increase in the error, whilst proportional control and both MPVC approaches decrease the error. MPVC 1 shows the most significant reduction (18%) in rise/fall error.

Absolute proportional overshoot/undershoot refers to the maximum error between profile and measured pressure for one second after the reference has initially been reached (green points in Fig. 8). PI and proportional control show a similar overshoot/undershoot metric while both MPVC approaches show a reduction with MPVC 2 showing the greatest reduction (24%).

VI. Discussion

The high median and mean values of MFA1-3 show that the model and the identification process can accurately model the healthy adult human response to pressure profiles whilst maintaining simplicity in design and efficiency in identification.

Inspection of the data revealed that most of the percentage accuracies below 75% were associated with reaction time (the

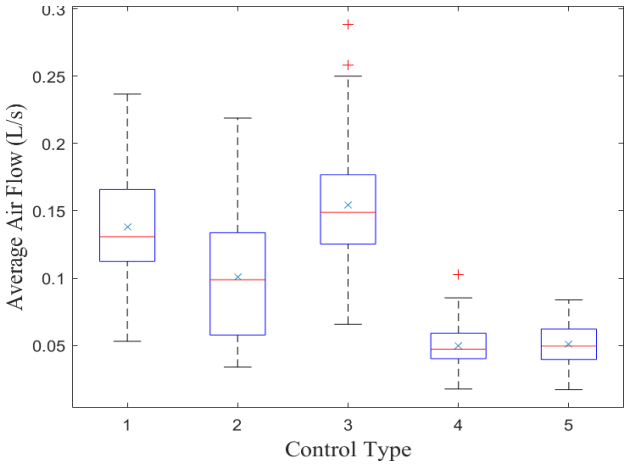

Fig. 14. Box and whisker plot of combined average airflow data for each control type. Control types are defined in Section V-B.

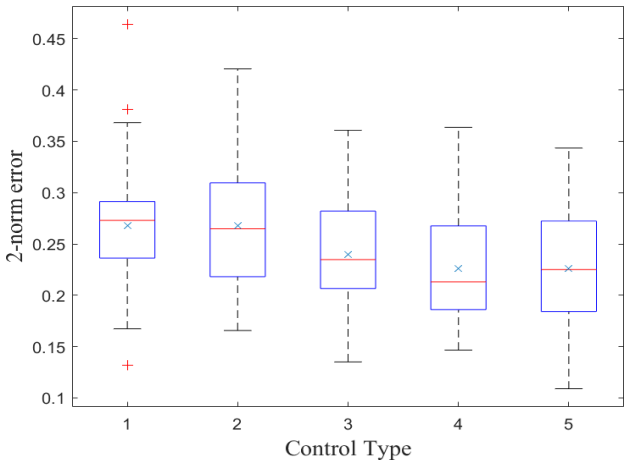

Fig. 15. Box and whisker plot of the combined error norm data for each control type

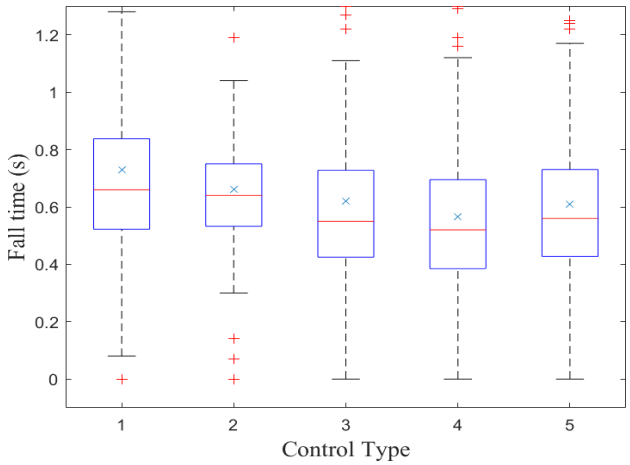

Fig. 16. Box and whisker of combined fall time data for each control type

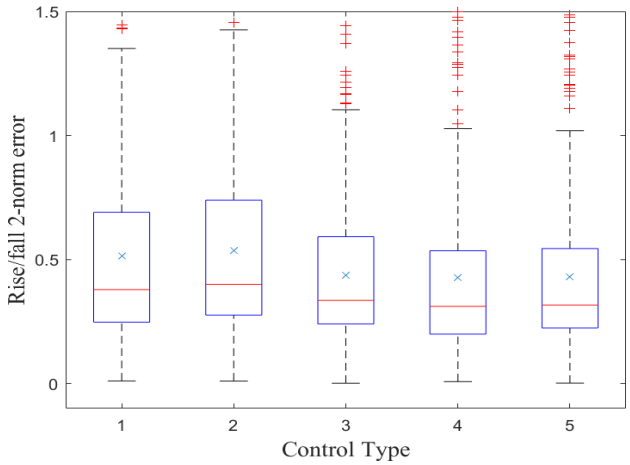

Fig. 17. Box and whisker of combined rise/fall 2-error norm data for each control type

combined perception and decision delays discussed in Section IV-B) to a step increase in the reference pofile. The model assumed a 0.3 second reaction time, and although most of the reaction delays were between 0.25 and 0.35, some were longer than 0.45 seconds. These longer reactions create a large error between measured and predicted output thus significantly reducing the prediction accuracy (e.g. see red crosses for P5 MFA3 and P7/P8 MFA2). This is an issue that can be easily resolved in future work by adding these delays into the identification process. These were not included in this work as the computational load would have been greatly increased, thus extending the identification time making it impractical with current hardware.

Across all metrics shown in Figs. 14-18, MPVC demonstrates a clear improvement in performance and tracking error over the existing clinical approach or use of proportional or PI control. Most significantly, it reduces the 2-norm of the tracking error by 22% and the absolute proportional overshoot/undershoot by 24%. This shows that the accuracy of the participants tracking ability both across the profile and in pressure changes is notably improved with assistance from MPVC. This confirms that the model, identification, and control method could be a viable approach to assist lung pressure profile tracking during TMD measurements.

An additional aspect to this study was the usability of the setup. The prevailing feedback received from the participants after testing was that with initial instructions the setup was easy to use and they understood what to do; they were mostly able to perform the intended actions (except those mentioned in Section IV-E); they found it easier to attain pressures (particularly higher pressures) with MPVC. This shows that the new setup and MPVC are successful both from a technical perspective as well as patient experience perspective.

VII. Conclusions and Future Work

Control of lung and airway pressure is a crucial component of research into ICP. It is needed for development of improved non-invasive measurement and diagnostic approaches to brain pathologies. This paper has presented the first control approach to assist airway pressure tracking. This employs a novel form of MPC which manipulates an internal parameter of a model rather than a control input. It controls the airflow out of a hand-held clinical breathing setup, via actuation of an integrated

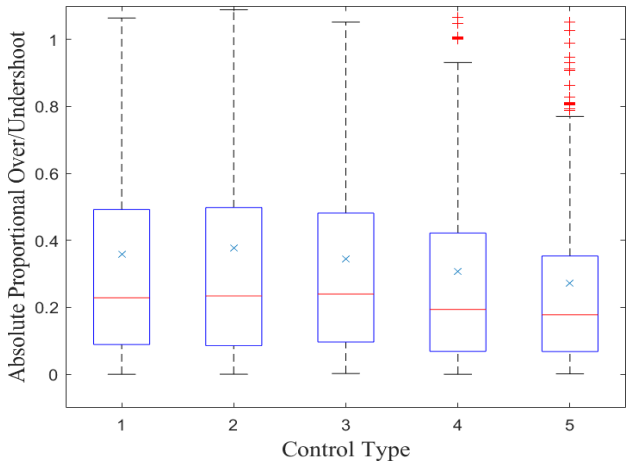

Fig. 18. Box and whisker of combined absolute proportional overshoot/undershoot data for each control type

valve, during lung pressure profile tracking. Results show that controlling airflow improves profile tracking by 22% compared to the original setup (Fig. 1). MPVC provides improved assistance across all metrics compared to the baseline and model-free control methods. MPVC was also accepted by participants in terms of usability.

This demonstrates that MPVC has a strong foundation and future work will validate its use in a clinical setting. Given the constraint that pressure cannot be actively increased, future work will focus on further reducing overshoot/undershoot across a more diverse range of participants. If the average value for proportional overshoot/undershoot could be reduced to below 0.2, MPVC would be an appropriate method to be applied, in a clinical setting, for lung pressure profiling alongside TMD measurements. Mechanisms to achieve this include: increasing the prediction horizon; increasing the number of valve resistances; incorporating reaction/delays into the set of identified parameters; and developing a multiple model adaptive control strategy to automatically adjust the model based on the reference pressure change.

References

[1] Brain Research UK, "Neurological facts," Online, 2024, accessed: April 23, 2024. [Online]. Available: https://www.brainresearchuk.org.uk/info/neuro-facts

[2] P. H. England, "Deaths associated with neurological conditions in england: 2001 to 2014," 2018.

[3] S. Gwer, V. Sheward, A. Birch, R. Marchbanks, R. Idro, C. R. Newton, F. J. Kirkham, J.-P. Lin, and M. Lim, "The tympanic membrane displacement analyser for monitoring intracranial pressure in children," *Child's Nervous System*, vol. 29, pp. 927–933, 2013.

[4] R. Marchbanks, "A study of tympanic membrane displacement," Ph.D. dissertation, Brunel University School of Engineering and Design PhD Theses, 1980.

[5] C. M. Campbell-Bell, A. A. Birch, D. Vignali, D. Bulters, and R. J. Marchbanks, "Reference intervals for the evoked tympanic membrane displacement measurement: a non-invasive measure of intracranial pressure," *Physiological Measurement*, vol. 39, no. 1, p. 015008, 2018.

[6] L. C. Finch, R. J. Marchbanks, D. Bulters, and A. A. Birch, "Refining non-invasive techniques to measure intracranial pressure: comparing evoked and spontaneous tympanic membrane displacements," *Physiological Measurement*, vol. 39, no. 2, p. 025007, 2018.

[7] S. Yildiz, S. Thyagaraj, N. Jin, X. Zhong, S. Heidari Pahlavian, B. A. Martin, F. Loth, J. Oshinski, and K. G. Sabra, "Quantifying the influence of respiration and cardiac pulsations on cerebrospinal fluid dynamics using real-time phase-contrast mri," *Journal of Magnetic Resonance Imaging*, vol. 46, no. 2, pp. 431–439, 2017.

[8] N. Sperna Weiland, J. Hermanides, M. Hollmann, B. Preckel, W. Stok, J. van Lieshout, and R. Immink, "Novel method for intraoperative assessment of cerebral autoregulation by paced breathing," *BJA: British Journal of Anaesthesia*, vol. 119, no. 6, pp. 1141–1149, 2017.

[9] R. L. Pasley, C. W. Leffler, and M. L. Daley, "Modeling modulation of intracranial pressure by variation of cerebral venous resistance induced by ventilation," *Annals of biomedical engineering*, vol. 31, no. 10, pp. 1238–1245, 2003.

[10] P. M. Lewis, J. V. Rosenfeld, R. Diehl, H. Mehdorn, and E. Lang, "Phase shift and correlation coefficient measurement of cerebral autoregulation during deep breathing in traumatic brain injury (tbi)," *Acta neurochirurgica*, vol. 150, no. 2, pp. 139–147, 2008.

[11] A. D. Guerci, A.-Y. Shi, H. Levin, J. Tsitlik, M. L. Weisfeldt, and N. Chandra, "Transmission of intrathoracic pressure to the intracranial space during cardiopulmonary resuscitation in dogs." *Circulation research*, vol. 56, no. 1, pp. 20–30, 1985.

[12] J. Gisolf, J. Van Lieshout, K. Van Heusden, F. Pott, W. Stok, and J. Karemaker, "Human cerebral venous outflow pathway depends on posture and central venous pressure," *The Journal of physiology*, vol. 560, no. 1, pp. 317–327, 2004.

[13] S. Dreha-Kulaczewski, A. A. Joseph, K.-D. Merboldt, H.-C. Ludwig, J. Gärtner, and J. Frahm, "Inspiration is the major regulator of human csf flow," *Journal of neuroscience*, vol. 35, no. 6, pp. 2485–2491, 2015.

[14] T. Ngubane, "Mechanical ventilation and the injured brain: refresher course," *Southern African Journal of Anaesthesia and Analgesia*, vol. 17, no. 1, pp. 76–80, 2011.

[15] M. C. Thompson, C. T. Freeman, N. O'Brien, A.-M. Hughes, T. Birch, and R. Marchbanks, "Model predictive valve control of lung pressure profile tracking," in *IEEE Australian & New Zealand Control Conference (ANZCC)*, 2022, pp. 132–137.

[16] G. Männel, C. Hoffmann, and P. Rostalski, "A robust model predictive control approach to intelligent respiratory support," in *IEEE Conference on Control Technology and Applications (CCTA)*, 2018, pp. 12–17.

[17] B. Hunnekens, S. Kamps, and N. Van De Wouw, "Variable-gain control for respiratory systems," *IEEE Transactions on Control Systems Technology*, vol. 28, no. 1, pp. 163–171, 2018.

[18] L. Hao, Y. Shi, M. Cai, S. Ren, Y. Wang, H. Zhang, and Q. Yu, "Dynamic characteristics of a mechanical ventilation system with spontaneous breathing," *IEEE Access*, vol. 7, pp. 172 847–172 859, 2019.

[19] A. C. Lua, K. C. Shi, and L. P. Chua, "Proportional assist ventilation system based on proportional solenoid valve control," *Medical engineering & physics*, vol. 23, no. 6, pp. 381–389, 2001.

[20] K. Y. Volyanskyy, W. M. Haddad, and J. M. Bailey, "Pressure-and work-limited neuroadaptive control for mechanical ventilation of critical care patients," *IEEE transactions on neural networks*, vol. 22, no. 4, pp. 614–626, 2011.

[21] S. Yan, H. Zhang, and L. Zihao, "Mechanical ventilation intelligent control technology based on fuzzy adaptive pid," in *2019 IEEE 8th International Conference on Fluid Power and Mechatronics (FPM)*. IEEE, 2019, pp. 156–163.

[22] B. Diong, A. Rajagiri, M. Goldman, and H. Nazeran, "The augmented ric model of the human respiratory system," *Medical & biological engineering & computing*, vol. 47, no. 4, pp. 395–404, 2009.

[23] B. Juroszek and J. Stanisławski, "Synthesis of the structure of the respiratory system in forced expiration," 2003.

[24] D. M. Wolpert, Z. Ghahramani, and J. R. Flanagan, "Perspectives and problems in motor learning," *TRENDS in Cognitive Sciences*, vol. 5, no. 11, pp. 487–494, 2001.

[25] H. Hazarika and A. Swarup, "Application of an optimal ilc algorithm for flow rate tracking of a ventilator system," in *2020 First IEEE International Conference on Measurement, Instrumentation, Control and Automation (ICMICA)*. IEEE, 2020, pp. 1–6.

[26] S. S. Oruganti Venkata, A. Koenig, and R. M. Pidaparti, "Mechanical ventilator parameter estimation for lung health through machine learning," *Bioengineering*, vol. 8, no. 5, p. 60, 2021.

[27] M. B. Rhudy, R. A. Salguero, and K. Holappa, "A kalman filtering tutorial for undergraduate students," *International Journal of Computer Science & Engineering Survey*, vol. 8, no. 1, pp. 1–9, 2017.

[28] G. R. Grice, R. Nullmeyer, and V. A. Spiker, "Human reaction time: Toward a general theory." *Journal of Experimental Psychology: General*, vol. 111, no. 1, p. 135, 1982.